Available online at www.sciencedirect.com
ScienceDirect
Ceramics International 35 (2009) 3201–3206
CERAMICS INTERNATIONAL
www.elsevier.com/locate/ceramint

Effects of preparation methods on the oxygen nonstoichiometry, B-site cation valences and catalytic efficiency of perovskite $La_{0.6}Sr_{0.4}Co_{0.2}Fe_{0.8}O_{3-\delta}$

Lei Ge [a], Zhonghua Zhu [b], Zongping Shao [a,*], Shaobin Wang [c], Shaomin Liu [c,**]

[a] State Key Laboratory of Materials-oriented Chemical Engineering, College of Chemistry & Chemical Engineering, Nanjing University of Technology, Nanjing 210009, PR China
[b] Division of Chemical Engineering, The University of Queensland, Brisbane, Queensland 4072, Australia
[c] Department of Chemical Engineering, Curtin University of Technology, Perth, WA 6845, Australia

Received 13 March 2009; received in revised form 31 March 2009; accepted 15 May 2009
Available online 18 June 2009

Abstract

$La_{0.6}Sr_{0.4}Co_{0.2}Fe_{0.8}O_{3-\delta}$ (LSCF) powders were synthesized respectively by an EDTA (ethylenediaminetetraacetic acid)–Citrate sol–gel process and a low-temperature auto-combustion process. The samples were characterized by XRD, SEM, BET, TGA and instant temperature analysis. The iodometric titration was used to determine the average valence of Co and Fe ions and the oxygen nonstoichiometry of the prepare powders. The catalytic properties of the synthesized powders were investigated by the hydrogen peroxide catalytic decomposition. Pure-perovskite structure was formed by both synthesis methods. The oxygen nonstoichiometry of the samples prepared by the auto-combustion process is larger than that by the sol–gel process. The catalytic activities of the powders from two synthesis processes also differed largely due to the different oxygen nonstoichiometry, surface area and crystalline sizes.

Keywords: $La_{0.6}Sr_{0.4}Co_{0.2}Fe_{0.8}O_{3-\delta}$; Oxygen nonstoichiometry; Hydrogen peroxide decomposition

1. Introduction

Perovskite oxides (ABO_3) displaying mixed ionic and electronic conducting (MIEC) properties at high temperatures have attracted much research interest for their potential use as membranes for air separation, catalytic membrane reactors for high temperature oxidations/gas partial oxidations, catalysts/membranes for clean combustion and electrode catalyst for solid oxide fuel cells (SOFC) [1–10]. Due to the mixed conducting properties, MIEC ceramic membranes can deliver 100% pure O_2 under the oxygen partial pressure gradient without the requirement of external electric loadings, offering the potential to replace the 100-year-old tonnage oxygen production technology via the expensive cryogenic route. Certainly, these oxygen selective membranes can find wider applications than solely in oxygen production since they can directly provide pure oxygen for many industrial processes where continuous supply of oxygen is needed. Applying MIEC perovskite oxides as electrodes in SOFC can greatly reduce the polarization resistance because of the high catalytic activity for oxygen reduction. $La_{0.6}Sr_{0.4}Co_{0.2}Fe_{0.8}O_{3-\delta}$ is a typical example of these perovskite materials and has been widely studied for these application purposes. Applications of these MIEC composite oxides always start with the high-quality powder synthesis and several methods like solid state reaction, freeze-drying, sol–gel, hydrothermal, co-precipitation and combustion of metal-organic precursors have been employed [11–20]. Among these methods, sol–gel and low temperature combustion are often cited as novel synthesis techniques for advanced applications. Different preparation methods may have influences on the parameters of the prepared perovskite powder properties in terms of valence state of B-site cations, values of oxygen nonstoichiometry (δ), oxygen vacancy concentration and so on. These parameters directly affect the

* Corresponding author. Tel.: +86 25 83172256; fax: +86 25 83172256.
** Corresponding author. Tel.: +61 8 92669056; fax: +61 8 92662681.
E-mail addresses: shaozp@njut.edu.cn (Z. Shao), shaomin.liu@curtin.edu.au (S. Liu).

0272-8842/$36.00
doi:10.1016/j.ceramint.2009.05.024

subsequent application performances like oxygen permeation and catalytic efficiency. In this work, we investigated the effects of two different synthesis methods (sol–gel and low temperature auto-combustion) on the valences of B site ions, the oxygen nonstoichiometry (δ) and catalytic efficiency in the decomposition of hydrogen peroxide. Perovskite $La_{0.6}Sr_{0.4}Co_{0.2}Fe_{0.8}O_{3-\delta}$ (LSCF) is selected for the target material of investigation.

2. Experimental

2.1. Powder preparation

(i) Low temperature auto-combustion

Cobalt nitrate, ferric nitrate, lanthanum nitrate, and strontium nitrate, all in analytical grades, were used as the metal sources. EDTA (ethylenediaminetetraacetic acid) powder and citric acid with purities higher than 99.5% were used as the chelants. Prior to the powder synthesis, the precise concentrations of all these nitrates were examined by EDTA titration technique. The mole ratio of EDTA and citric acid to metal ions in this study was fixed at 1:2:1. EDTA powder was added into aqueous ammonium hydroxide to form a water-soluble ammonium salt. Stoichiometric amounts of metal nitrates were dissolved in distilled water. The required amount of EDTA, citric acid, and NH_4NO_3 for the preparation of 0.005 mol LSCF was introduced in sequence into the nitrate solution under stirring condition. The mixed solution was then heated at 90 °C over a hot plate under magnetic stirring until a gel was formed, which was cooled down to room temperature and then transferred to a pre-heated oven at 250 °C for auto-combustion. The auto-combustion experiment was conducted within a 250 mL Pyrex beaker. An electrical fan was used during the heat treatment to ensure a homogeneous temperature distribution and to enhance the gas flow inside the oven.

(ii) Sol–gel synthesis

The typical EDTA–citrate complexing process can be found elsewhere [21]. Briefly, the necessary amount of EDTA (dissolved in ammonia solution) was added into the mixed metal nitrate solution, followed by the addition of solid citric acid with mole ratio of total metal ions to EDTA and citrate is 1:1:2. The gel was obtained by thickening the final solution at 90 °C on a hot plate under stirring condition. Subsequently, the gel was pyrolysed at 250 °C and further calcinated at 900 °C for 5 h to get the final powder product.

2.2. Characterization

During combustion process, a thermocouple was immersed into the gel to measure the temperature around the powder. Yudian 708P temperature indictor with Labview program was used to monitor the temperature–time profiles of the auto-combustion process at the sampling rate of 10 point per second [22–23]. The lattice structure of the synthesized powders was determined by X-ray diffraction (XRD, Bruker D8 Advance) using Cu Kα radiation. The diffraction patterns were collected at room temperature by step scanning in the range of $10 \leq 2\theta \leq 90^{\circ}$. The weight loss of the samples was examined by the Thermal Gravity Analysis (TGA) using a NETZSCH STA 409 thermal gravity analyzer under flowing air atmosphere at the rate of 10 mL min^{-1}. Twenty-milligram sample was applied for this analysis. The specific surface area of the oxide powders was characterized by N_2 adsorption using a BELSORP II instrument. Before the measurement, the samples were pre-treated at 200 °C for 2 h under vacuum to remove the surface adsorbed species. The morphologies of the powders were examined using an Environmental Scanning Electron Microscopy (ESEM, QUANTA-2000). The elemental compositions of the powder were confirmed by the energy dispersive X-ray (EDX) spectrometer attached to the ESEM instrument. The stoichiometry of oxygen vacancies was measured with the iodometric titration technique [24]. Samples were dissolved in a solution of potassium iodide in HCl and heated in an oxygen-free environment. The iodide reduced any B-site ions (B^{3+}, B^{4+}) present to B^{2+} and was simultaneously oxidized to form I_2. The amount of I_2 released was quantified via redox titration with thiosulfate. The oxygen vacancy stoichiometry was calculated based on the amount of I_2 formed.

2.3. Catalytic efficiency test

The catalytic efficiency of the prepared perovskite powder was tested by decomposing the peroxide hydrogen. For this purpose, 7.5 mL H_2O_2 solution (0.2 mol/L) was added into 30 mL NaOH solution (6 mol/L) and 50 mg perovskite powder was subsequently added inside the reactant solution. The reaction rate was measured by the production rate of oxygen at room temperature (298 K). The hydrogen peroxide decomposition reaction can be expressed as [25,26]:

$$HO_{2(aq)}{}^{-} \rightarrow \tfrac{1}{2}O_2 + OH^{-}_{(aq)} \quad (1)$$

The concentration change of $HO_2{}^{-}$ with time is calculated based on Eq. (2):

$$C_{HO_2{}^{-}} = C_0 - \left[\frac{2P_{O_2}V_{O_2}}{RTV_s}\right] \quad (2)$$

where C_0 is the initial concentration of $HO_2{}^{-}$, P_{O_2} is the O_2 partial pressure corrected for water vapor pressure, V_{O_2} is the volume (mL) of O_2 production vs. time (second), V_s is the volume of solution. The rate constant k_w can be calculated as:

$$k_w = \frac{d(\ln C_{HO_2{}^{-}})/dt}{m} \quad (3)$$

where m is the weight of catalyst.

3. Results and discussion

3.1. LSCF powder synthesis

In this study, LSCF composite oxide powders were prepared using EDTA–citrate sol–gel and low-temperature auto-com-

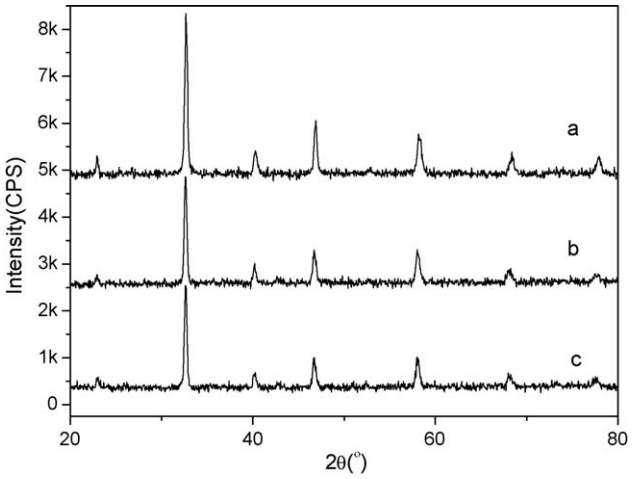

Fig. 1. XRD patterns of the as-prepared powders (a: normal sol–gel method; b: auto-combustion synthesis with 25 g NH_4NO_3; c: combustion synthesis with 35 g NH_4NO_3).

bustion methods. Calcination at 900 °C for at least 5 h is necessary for the sol–gel method to form the well-crystallized pure perovskite phase without carbon residue contamination [21]. By contrast, the LSCF powder from auto-combustion process is simple and fast. According to the amount of the combustion trigger (NH_4NO_3) addition, the combustion types and the maximum flame temperature may vary; and therefore lead to different powder properties [22–23] which will be further discussed below. Here, two typical samples with different NH_4NO_3 addition were comparatively investigated. For clarity purpose, the samples from the normal EDTA–citrate method and the auto-combustion processes with lower (25 g) and higher (35 g) contents were denoted as samples a, b and c, respectively. Fig. 1 shows the XRD pattern of the as-obtained powders. All the samples showed pure perovskite structure with good crystallization. The grain sizes of these samples calculated by Scherer Equation was 21.2 nm (a), 22.5 nm (b) and 23.8 nm (c), respectively. Fig. 2 is the SEM pictures for the three samples. As can be seen, sample a has the smallest grain size with more uniform particle morphology; samples b and c have relatively larger sizes and are more aggregated with hollow structure associated with the fast combustion behavior and fast gas release. Chemical composition analyses via EDX shows that the atomic ratio of the powder is in excellent agreement with the strict stoichiometry of $La_{0.6}Sr_{0.4}Co_{0.2}Fe_{0.8}O_{3-\delta}$.

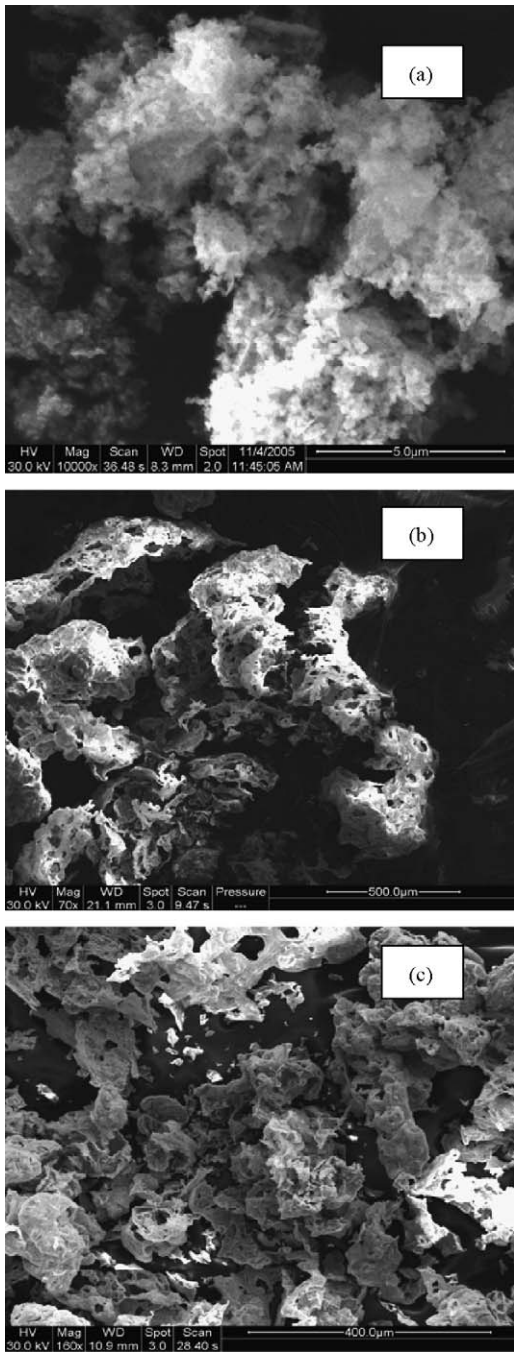

Fig. 2. SEM images of the powder synthesized from normal EDTA–citrate process (a) and the auto-combustion process with various NH_4NO_3 amount (b: 25 g, c: 35 g).

3.2. Oxygen nonstoichiometry

For $La_{1-x}Sr_xCo_{1-y}Fe_yO_{3-\delta}$ perovskite, the oxygen nonstoichiometry (δ) is related to many factors i.e. the Sr (A-site cation) content, the B-site cation valence state and surrounding environment (temperature and oxygen partial pressure) [3,27–28]. The oxygen vacancy concentration ($[V_o^{\cdot\cdot}]$) determined by δ is an important parameter which is associated with many important properties including ionic/electronic conductivity, oxygen transport behavior and catalytic activity. For $La_{0.6}Sr_{0.4}Co_{0.2}Fe_{0.8}O_{3-\delta}$, the content and valence of A-site cations are fixed, the oxygen nonstoichiometry change is mainly reflected by the variation of B-site cation valence state. The oxygen nonstoichiometry δ of the samples derived by different synthesis processes were measured at room temperature via iodometric titration technique. Table 1 shows the results of the three LSCF powders from two different routes. It can be seen clearly that LSCF powder derived from auto-combustion process showed lower B-site cation valences and thus higher oxygen vacancy concentration. This phenomenon can be explained from the features of the auto-combustion. The final powder from

Table 1
The average valence of Co and Fe ions, the oxygen nonstoichiometry and reaction kinetic constant of H_2O_2 decomposition with LSCF catalysts.

Samples	Synthesis method	The average valence of Co and Fe	Oxygen nonstoichiometry (δ)	$k_w \times 10^3$ (g^{-1} s^{-1})
a	Sol–gel and heated at 900 °C	3.47	−0.034	30.4
b	Auto-combustion with lower NH_4NO_3 content	3.34	0.028	5.8
c	Auto-combustion with higher NH_4NO_3 content	3.29	0.055	3.6
d	Sample b re-heated at 700 °C	3.47	−0.034	16.9
e	Sample c re-heated at 700 °C	3.48	−0.040	6.4

combustion was synthesized in a very fast way during which the product went through a high flame temperature but the time is too short for B-site cations to be sufficiently oxidized. Fig. 3 shows the evidence of temperature difference between the two combustion processes. As can be seen, the temperature of powder-c was more than 700 °C and dropped sharply to 300 °C in 2 min. The fast cooling of the powder can be considered as special quenching process which keeps the B-site cation in the lower valence state resulted from the high temperature environment. On the other hand, the auto-combustion process is an oxygen consuming reaction accompanying with the release of a large amount of gases, such as N_2 and H_2O. These releasing gases diluted the oxygen partial pressure during the quick high temperature treatment, which also contributed to the higher oxygen vacancy concentration. Therefore, it is reasonable to see that lower B-site ion valence and more oxygen vacancy were created in the samples from combustion. To further oxidize the B-site cations, samples b and c were treated in air at 700 °C again for a few hours before slowly cooling down to room temperature. These two re-heated samples were signed as d and e, respectively, with result showing in Table 1. Obviously, after heat treatment, the oxygen nonstoichiometry was reduced by increasing the average valence of Co and Fe ions and absorbing oxygen into lattice. It is interesting to note that the B-valences of the re-heated samples were almost equal to sample-a for normal EDTA–citrate method.

Thermogravimetric analysis was used to further investigate the oxygen vacancy difference. Fig. 4 shows the sample weight loss profile in air atmosphere with temperature change. Sample-a displays a steady weight lose at temperatures less than 700 °C, which can be explained as the lattice oxygen desorption caused by the thermal reduction of Co^{4+} and Fe^{4+} to Co^{3+} and Fe^{3+}. At temperature between 700 and 1000 °C, the further thermal reduction of Co^{3+} to Co^{2+} led to a dramatic weight loss accounting for 2%. However, samples b and c showed different trends as shown in Fig. 4 b and c. They experienced slight weight increment before the first thermal reduction at around 400 °C. According to iodometric titration results, samples b and c have B-site cations with lower valences and were re-oxidized in air and therefore the weight initially increased. Due to the lowest initial B-site cation valences, the final weight loss for sample-c was the smallest. However, samples a and b showed a similar final weight loss percentage although sample-b has lower B-cation valence at room temperature. One possible reason is that sample-b from auto-combustion with less NH_4NO_3 addition and a lower combustion temperature (as shown in Fig. 3) has minor carbon residue; therefore the larger weight loss of sample-b in Fig. 4 is also due to the burning out of the carbon. However, because of the higher content of NH_4NO_3, sample-c experienced more intensified combustion which completely removed the carbon residue [22–23].

3.3. Hydrogen peroxide catalytic properties

The catalytic activity of powder derived from two different methods was examined by the decomposition of peroxide

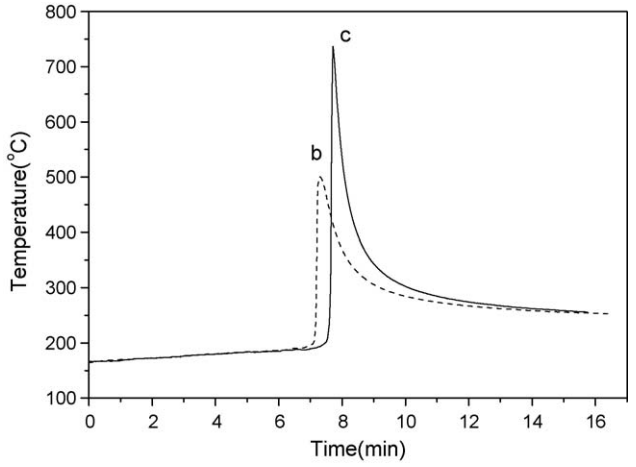

Fig. 3. Temperature–time profiles for the preparation of 0.005 mol LSCF via combustion synthesis method (b: auto-combustion synthesis with 25 g NH_4NO_3; c: combustion synthesis with 35 g NH_4NO_3).

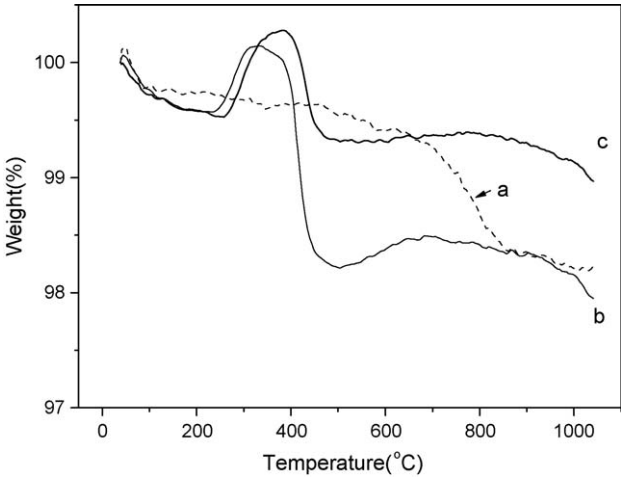

Fig. 4. TG profiles of the as-prepared LSCF via normal sol–gel method (a) and combustion synthesis method (NH_4NO_3 b: 25 g, c: 35 g).

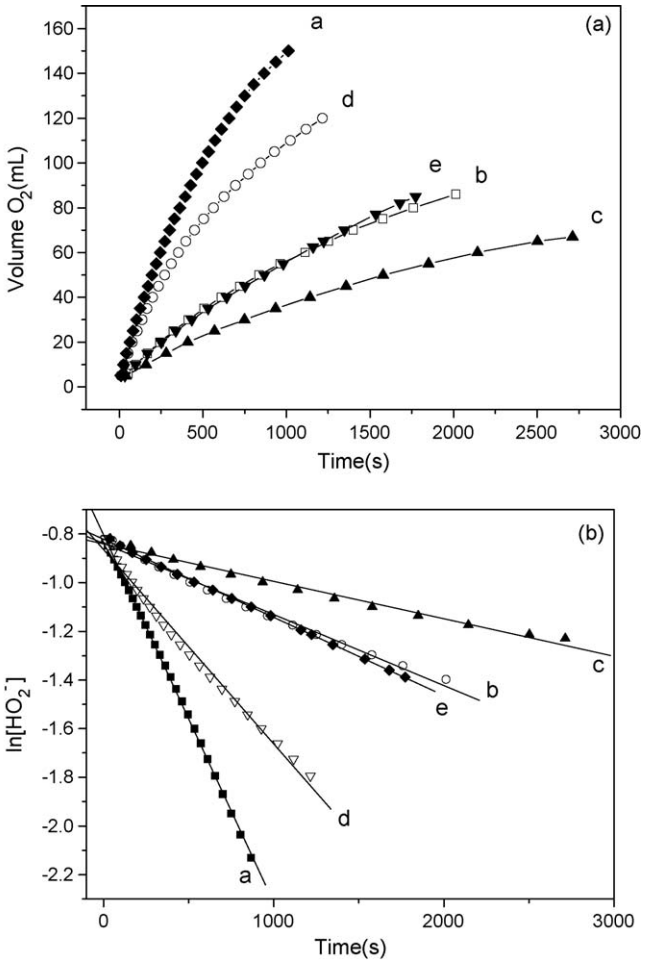

Fig. 5. (a) the curve for the decomposition of H_2O_2; (b) the curve of ln [HO_2^-] to time (a: normal sol–gel method; b: auto-combustion synthesis with 25 g NH_4NO_3; c: combustion synthesis with 35 g NH_4NO_3; d and e: b and c after re-sintering at 700 °C).

hydrogen. In addition to the normal sol–gel process, the samples from the auto-combustion with and without 700 °C treatment were also investigated for comparison purposes. The typical reaction profiles of the time dependences of oxygen production and HO_2^- concentration are shown in Fig. 5. The reaction kinetic constant of H_2O_2 decomposition catalyzed by LSCF powders is shown Table 1. It is clear that sample-a performed best in H_2O_2 decomposition evidenced by the most rapid oxygen production rate, the highest rate of HO_2^- concentration decrease or the largest kinetic constant. Obviously, samples from auto-combustion have a lower catalytic activity, but can be enhanced by further treatment at 700 °C.

Several important factors affecting the catalytic H_2O_2 decomposition rate are: (i) active surface area, (ii) variable surface concentrations of active sites related to B-site cation valences of the perovskite catalyst, (iii) oxygen vacancy concentration and (iv) surface morphology of the catalyst. Based on BET test results, sample a shows highest specific surface area ($3.6\ m^2\ g^{-1}$) followed by samples b and c ($1.8\ m^2\ g^{-1}$). The lower surface area of samples b and c is due to over-heat-treatment taking place during the combustion [22]. As shown in Fig. 3, samples b and c experienced high temperatures of 500 and 700 °C, respectively. However, due to the temperature refection delay by the thermocouple signaling, the real temperatures for these two powders during combustion may be far higher than that. Previous work indicated that higher concentration of fully oxidized transition metal sites in the perovskite would increase the number of active constituents involved in the catalytic decomposition of H_2O_2 [26–30]. During the decomposition process, the electron is transferred from the B-site ion to an oxidized site on the surface of the catalyst to produce HO_2^- radical. In LSCF composite oxide, Co^{3+}, Co^{4+} and Fe^{4+} are mainly expected to be the active sites for hydrogen peroxide decomposition and their concentration can be changed through different synthesis routes. By contrast, sample a has higher average valence of B-site cations. Therefore it is not difficult to understand that samples b and c from auto-combustion showed lower catalytic efficiency. After heat treatment in air, their catalytic behavior has been improved due to the oxidation of B-site cations giving rise to more active site for the reaction. Therefore, for catalysis application, the auto-combustion synthesis should be connected with post-heat-treatment for re-oxidizing B-site cations to improve the activity.

4. Conclusions

$La_{0.6}Sr_{0.4}Co_{0.2}Fe_{0.8}O_{3-\delta}$ was synthesized by normal EDTA–citrate sol–gel process and low-temperature auto-combustion process with NH_4NO_3 as the combustion trigger. All the samples showed pure perovskite structure with good crystallization. LSCF powder from sol–gel process with higher surface area shows higher B-site cation valences and better catalytic properties. LSCF powders from auto-combustion process have lower valences of B-site cations and higher oxygen nonstoichiometry due to rapid combustion time and fast cooling rate. Powder from auto-combustion process showed a re-oxidation process in air at relative low temperature. Based on hydrogen peroxide decomposition results, the optimum auto-combustion mode with lower combustion trigger and post-calcination of as-prepared powder should be employed to enhance the better catalytic property if the powder application is for catalysis.

Acknowledgements

This work was supported by the National Basic Research Program of China under contract No. 2007CB209704. The authors gratefully acknowledge the financial support from the Australian Research Council for the project of DP0985578.

References

[1] H.J.M. Bouwmeester, A.J. Burggraaf, Dense ceramic membranes for oxygen separation, in: A.J. Burggraaf, L. Cot (Eds.), Fundamentals of Inorganic Membrane Science and Technology, Elsevier, Amsterdam, 1996, p. 435.

[2] Y. Teraoka, H. Zhang, S. Furukawa, N. Yamazoe, Oxygen permeation through perovskite-type oxides, Chem. Lett. 11 (1985) 1743–1746.
[3] Y. Teraoka, H. Zhang, K. Okamoto, N. Yamazoe, Mixed ionic-electronic conductivity of $La_{1-x}Sr_xCo_{1-y}Fe_yO_{3-\delta}$, Mater. Res. Bull. 23 (1988) 51–58.
[4] A. Petric, P. Huang, F. Tietz, Evaluation of La–Sr–Co–Fe–O perovskites for solid oxide fuel cells and gas separation membranes, Solid State Ionics 135 (2000) 719–725.
[5] T. Hibino, A. Hashinmoto, T. Inoue, J. Tokuno, S. Yoshida, M. Sano, A low operating-temperature solid oxide fuel cell in hydrocarbon-air mixtures, Science 288 (2000) 2031–2033.
[6] Z.P. Shao, S.M. Haile, J. Ahn, P.D. Ronney, Z.L. Zhan, S.A. Barnett, A thermally self-sustained micro solid-oxide fuel-cell stack with high power density, Nature 435 (2005) 795–798.
[7] Z.P. Shao, S.M. Haile, A high-performance cathode for the next generation of solid-oxide fuel cells, Nature 431 (2004) 170–173.
[8] Y.S. Lin, Y. Zeng, Catalytic properties of oxygen semipermeable perovskite-type ceramic membrane materials for oxidative coupling of methane, J. Catal. 164 (1996) 220–231.
[9] S.P.S. Badwal, F.T. Ciacchi, Ceramic membrane technologies for oxygen separation, Adv. Mater. 13 (2001) 993–996.
[10] J.E. ten Elshof, H.J.M. Bouwmeester, H. Verweij, Oxidative coupling of methane in a mixed-conducting perovskite membrane reactor, Appl. Catal. A. 130 (1995) 195–212.
[11] M.P. Pechini, U.S. Patent 3,330,697 (1967).
[12] A. Kwiatkowski, K. Reszka, A. Szymanski, Preparation of corundum and steatite ceramics by the freeze-drying method, Ceram. Int. 11 (1985) 143.
[13] S.P. Gaikwad, H.S. Potdar, V. Violet Samuel, Ravi, Co-precipitation method for the preparation of fine ferroelectric $BaBi_2Nb_2O_9$, Ceram. Int. 31 (2005) 379–381.
[14] K.A. Singh, L.C. Pathak, S.K. Roy, Effect of citric acid on the synthesis of nano-crystalline yttria stabilized zirconia powders by nitrate-citrate process, Ceram. Int. 33 (8) (2007) 1463–1468.
[15] Y.B. Xu, X. Yuan, P.X. Lu, G.H. Huang, C.L. Zeng, Synthesis of $La(Mg_{1/2}Ti_{1/2})O_3$ powder through ethylenediaminetetraacetic acid gel combustion, Ceram. Int. 32 (1) (2006) 57–60.
[16] Y.G. Wang, G. Xu, L.L. Yang, Z.H. Ren, X. Wei, W.J. Weng, P.Y. Du, G. Shen, G.R. Han, Hydrothermal synthesis of single-crystal bismuth ferrite nanoflakes assisted by potassium nitrate, Ceram. Int. 35 (3) (2009) 1285–1287.
[17] S.J. Qiu, X.D. Zheng, C. Gao, X.X. Gan, J. Chen, C. Yang, H.Q. Fan, $Pb(Zr_{0.95}Ti_{0.05})O_3$ powders and porous ceramics prepared by one-step pyrolysis process using non-aqueous Pechini method, Ceram. Int. 35 (3) (2009) 733–740.
[18] W. Zhou, Z.P. Shao, R. Ran, W.Q. Jin, N.P. Xu, Functional nanocomposite oxides synthesized by environmental-friendly auto-combustion within a micro-bioreactor, Mater. Res. Bull. 43 (8–9) (2008) 2248–2259.
[19] D.G. Lamas, R.E. Juarez, G.E. Lascalea, N.E.W. de Reca, Synthesis of compositionally homogeneous, nanocrystalline ZrO_2-35 mol% CeO_2 powders by gel-combustion, J. Mater. Sci. Lett. 20 (2001) 1447–1449.
[20] J. Sunarso, S. Baumann, J.M. Serra, W.A. Meulenberg, S. Liu, Y.S. Lin, J.C. Diniz da Costa, Mixed ionic–electronic conducting (MIEC) ceramic-based membranes for oxygen separation, J. Membr. Sci. 320 (2008) 13–41.
[21] W. Zhou, Z.P. Shao, W.Q. Jin, Synthesis of nanocrystalline conducting composite oxides based on a non-ion selective combined complexing process for functional applications, J. Alloys Compd. 426 (2006) 368–374.
[22] L. Ge, W. Zhou, R. Ran, Z.P. Shao, S.M. Liu, Facile auto-combustion synthesis of $La_{0.6}Sr_{0.4}Co_{0.2}Fe_{0.8}O_{3-\delta}$ (LSCF) perovskite via a modified complexing sol–gel process with NH_4NO_3 as combustion aid, J. Alloys Compd. 450 (2008) 323–329.
[23] L. Ge, R. Ran, W. Zhou, Z.P. Shao, S.M. Liu, W.Q. Jin, N.P. Xu, Facile auto-combustion synthesis for oxygen separation membrane application, J. Membr. Sci. 329 (2009) 219–227.
[24] G.H. Jonker, J.H. Van Santen, Magnetic compounds with perovskite structure III. Ferromagnetic compounds of cobalt, Physica 19 (1953) 120–130.
[25] S.P. Jiang, Z.G. Lin, A.C. Tseung, Homogeneous and heterogeneous catalytic reactions in cobalt oxide/graphite air electrodes. I. Chemical kinetics of peroxide decomposition by Co(II) ions in alkaline solutions, J. Electrochem. Soc. 137 (3) (1990) 759–764.
[26] A. Ariafard, H.R. Aghabozorg, F. Salehirad, Hydrogen peroxide decomposition over $La_{0.9}Sr_{0.1}Ni_{1-x}Cr_xO_3$ perovskites, Catal. Commun. 4 (2003) 561–566.
[27] E. Bucher, W. Sitte, G.B. Caraman, V.A. Cherepanov, T.V. Aksenova, M.V. Ananyev, Defect equilibria and partial molar properties of $(La,Sr)(Co,Fe)O_{3-\delta}$, Solid State Ionics 177 (2006) 3109–3115.
[28] D. Mantzavinos, A. Hartley, I.S. Metcalfe, M. Sahibzada, Oxygen stoichiometries in $La_{1-x}Sr_xCo_{1-y}Fe_yO_{3-\delta}$ perovskites at reduced oxygen partial pressures, Solid State Ionics 134 (2000) 103–109.
[29] H. Falcón, R.E. Carbonio, J.L.G. Fierro, Correlation of oxidation states in $LaFe_xNi_{1-x}O_{3+\delta}$ oxides with catalytic activity for H_2O_2 decomposition, J. Catal. 203 (2001) 264–272.
[30] N.A.M. Deraz, Catalytic decomposition of H_2O_2 on promoted cobaltic oxide catalysts, Mater. Lett. 57 (2002) 914–920.